Supporting Information

Design of Narrow Bandgap Non-Fullerene Acceptors for Photovoltaic Applications and Investigation of Non-Geminate Recombination Dynamics

*Joachim Vollbrecht, Jaewon Lee, Seo-Jin Ko, Viktor V. Brus, Akchheta Karki, William Le, Martin Seifrid, Michael J. Ford, Kilwon Cho, Guillermo C. Bazan, Thuc-Quyen Nguyen**

Dr. J. Vollbrecht, Dr. J. Lee, Dr. V. V. Brus, A. Karki, W. Le, Dr. M. Seifrid, Dr. M. J. Ford, Prof. G. C. Bazan, Prof. T.-Q. Nguyen
Center for Polymers and Organic Solids
Departments of Chemistry and Biochemistry
University of California at Santa Barbara
Santa Barbara, CA 93106, USA
E-mail: quyen@chem.ucsb.edu

Dr. J. Lee, Prof. K. Cho
Center for Advanced Soft Electronics
Department of Chemical Engineering
Pohang University of Science and Technology
Pohang, 37673, Republic of Korea

Dr. S.-J. Ko
Division of Advanced Materials,
Korea Research Institute of Chemical Technology (KRICT)
Daejeon 34114, Republic of Korea

This paper is dedicated to Professor Tobin Marks on the occasion of his 75th birthday.

Keywords: organic photovoltaics, non-fullerene acceptors, near-infrared optoelectronics, narrow bandgap acceptors, non-geminate recombination

1. Materials and Methods

Materials All reagents and chemicals were purchased from commercial sources and used without further purification. All anhydrous organic solvents for the synthesis, characterization, and device fabrication steps were purchased from Sigma-Aldrich and TCI. Compound 4, compound 6, COTIC-4F, and CTIC-4F were prepared *via* a modified synthetic condition from literatures.[1-4] CETIC-4F, like CTIC-4F and COTIC-4F, is soluble at room temperature in common organic solvents, such as dichloromethane, chloroform, and chlorobenzene.

Characterizations of compounds ^{1}H and ^{13}C NMR spectra of intermediate monomers were recorded on a **Varian Unity Inova 500 MHz spectrometer** in deuterated chloroform solution ($CDCl_3$) with 0.003%TMS as internal reference. Mass spectra were obtained from Bruker Microflex Matrix-Assisted LASER Desorption Ionization - Time of Flight Mass Spectrometer (MALDI-TOF) using 1,8-Dihydroxy-9(10H)-anthracenone (Dithranol) as a matrix recorded in a (+)-reflector mode. Elementary analysis was carried out using a CE440 elemental analyzer. Ultraviolet-Visible-Near-infrared (UV-Vis-NIR) absorption spectra were recorded on a Perkin Elmer Lambda 750 spectrophotometer. For the measurements of thin films, materials were spun coated onto precleaned glass substrates from chloroform solutions (10 mg mL^{-1}). Optical band gap (Eg^{opt}) was determined from the absorption onset of thin film sample.

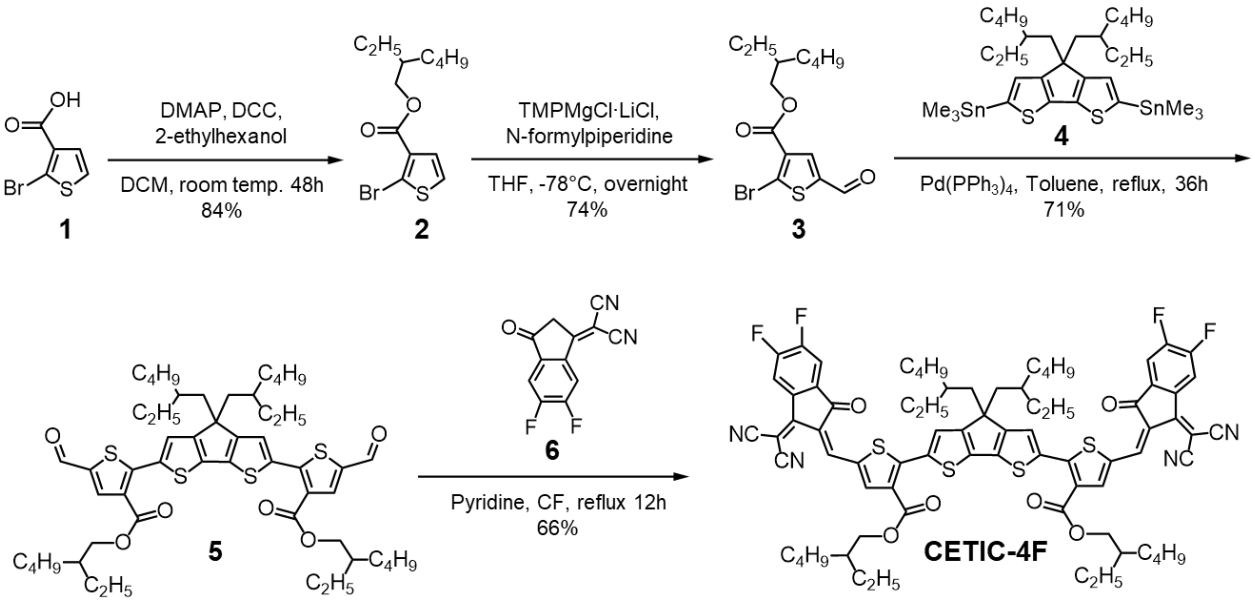

Scheme S1. Synthetic procedures of CETIC-4F.

2-Ethylhexyl 2-bromothiophene-3-carboxylate (compound 2): To a solution of 2-bromothiophene-3-carboxylic acid (10.0 g, 48.3 mmol) in 40 mL of dry dichloromethane (DCM) were added 4-(dimethylamino)pyridine (DMAP) (2.1 g, 16.9 mmol, 0.35 equiv) and 2-ethylhexanol (9.9 g, 96.6 mmol, 2 equiv). The flask was purged with N_2 for 20 min and N,N′-dicyclohexylcarbodiimide (DCC) (11.0 g, 53.1 mmol, 1.1 equiv) was added. The mixture was allowed to stir at room temperature for 48 hours. Precipitated urea was filtered off, and the filtrate was concentrated in vacuum. The residue was purified by silica gel column chromatography (*n*-hexane/DCM, 1/1) to afford the product as a colorless oil (13.0 g, 84%).

^{1}H NMR (500MHz, $CDCl_3$, ppm): δ 7.36 (d, 1H), 7.21 (d, 1H), 4.21 (m, 2H), 1.69 (m, 1H), 1.26 – 1.53 (m, 8H), 0.86 – 0.95 (m, 6H).

2-Ethylhexyl 2-bromo-5-formylthiophene-3-carboxylate (compound 3): To a flame-dried and nitrogen-filled one-neck round-bottom flask, compound 2 (3.2 g, 10.0 mmol) was dissolved in 15 mL of THF and cooled down to −78 °C. A 1 M solution of 2,2,6,6-tetramethylpiperidinylmagnesium chloride−lithium chloride complex (TMPMgCl·LiCl) in THF (13.0 mL, 13.0 mmol) was added dropwise under N_2. The mixture was kept at −78 °C for 3.5 h before N-formylpiperidine (2.8 mL, 25.0 mmol) was added. The reaction mixture was allowed to warm up to room temperature and stirred overnight. After extraction with dichloromethane and water, the organic layer was dried over $MgSO_4$ and concentrated in vacuum. The residue was purified by silica gel column chromatography (*n*-hexane/dichloromethane, 5:5, Rf = 0.45) to afford the product as a yellowish oil (356 mg, 74%). ^{1}H NMR (500MHz, $CDCl_3$, ppm): δ 9.81 (s, 1H), 7.98 (s, 1H), 4.25 (m, 2H), 1.70 (m, 1H), 1.23 – 1.50 (m, 8H), 0.85 – 0.96 (m, 6H).

Bis(2-ethylhexyl)-2,2'-(4,4-bis(2-ethylhexyl)-4H-cyclopenta[1,2-b:5,4-b']dithiophene-2,6-diyl)bis(5-formylthiophene-3-carboxylate) (compound 5): A mixture of compound 4 (360 mg, 0.49 mmol), compound 3 (450 mg, 1.30 mmol, 2.6 eq), ($Pd(PPh_3)_4$) (25 mg), and dry toluene:DMF (20:5 mL) was added into a flame-dried and nitrogen-filled one-neck round-bottom flask (50 mL). The flask was purged with N_2 for 20 min and the reactant was heated to 120 °C for 48 h. After the mixture cooled to room temperature, DI water was added, and the mixture was extracted with dichloromethane two times (50 ml×3). The organic layer was dried over $MgSO_4$ and concentrated in vacuum. The residue was purified by silica gel column

chromatography (*n*-hexane/dichloromethane, 2:8) to afford the product as a sticky red solid (337 mg, 73%). ^{1}H NMR (500MHz, $CDCl_3$, ppm): δ 9.86 (s, 2H), 8.07 (s, 2H), 7.69 (t, 2H), 4.25 (m, 4H), 1.95 (m, 4H), 1.73 (m, 2H), 1.30 – 1.50 (m, 18H), 0.87 – 1.05 (m, 28H), 0.60 – 0.74 (m, 12H).

Bis(2-ethylhexyl)-2,2'-(4,4-bis(2-ethylhexyl)-4H-cyclopenta[1,2-b:5,4-b']dithiophene-2,6-diyl)bis(5-((Z)-(1-(dicyanomethylene)-5,6-difluoro-3-oxo-1H-inden-2(3H)-ylidene)methyl)thiophene-3-carboxylate) (CETIC-4F): A mixture of compound 5 (175 mg, 0.19 mmol) and 2-(5,6-difluoro-3-oxo-2,3-dihydro-1H-inden-1-ylidene)malononitrile, compound 6, (160 mg, 0.70 mmol, 3.6 eq), dry chloroform (20 mL), and pyridine (0.4 mL) was added into to a flame-dried and nitrogen-filled one-neck round-bottom flask (50 mL). The flask was purged with N_2 for 10 min and the reactant was heated to 60 °C for 12 h. After the mixture cooled to room temperature, the reaction mixture was concentrated in vacuum. The residue was purified by silica gel column chromatography (*n*-hexane/dichloromethane, 2:8) to afford the product as a dark brown solid (178 mg, 70%). ^{1}H NMR (500MHz, $CDCl_3$, ppm): δ 8.76 (s, 2H), 8.57 (q, 2H), 8.16 (s, 2H), 7.93 (t, 2H), 7.74 (m, 2H), 4.28 (d, 4H), 2.01 (m, 4H), 1.79 (m, 2H), 1.28 – 1.50 (m, 16H), 0.87 – 1.09 (m, 28H), 0.62 – 0.78 (m, 12H).

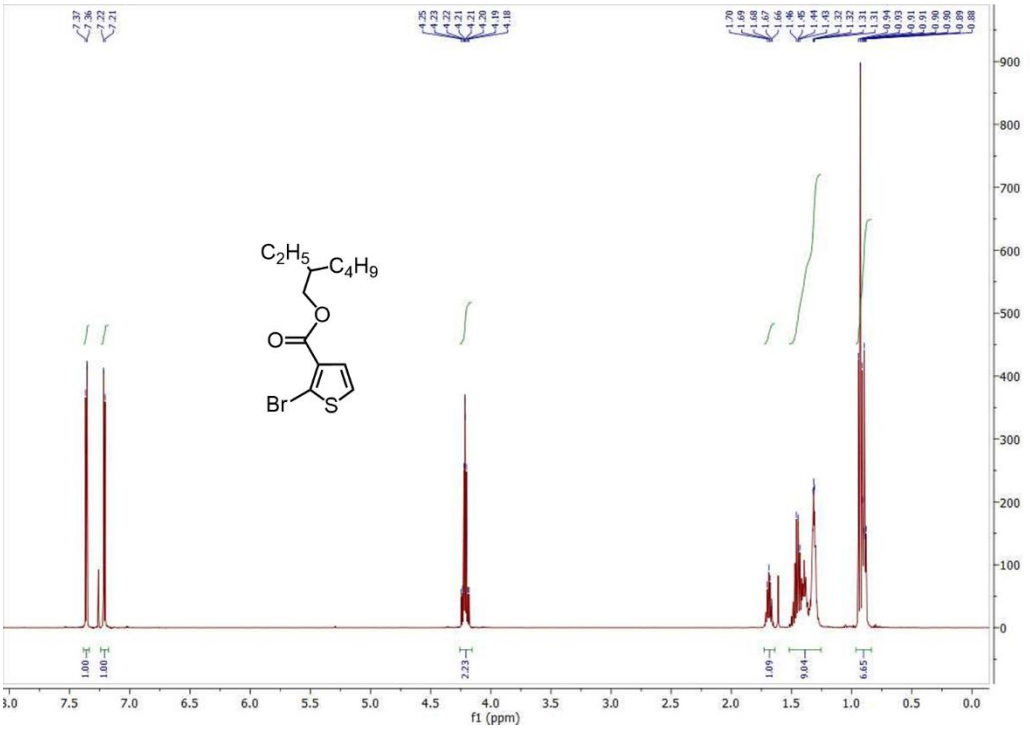

Figure S1. ^{1}H NMR spectrum of compound 2.

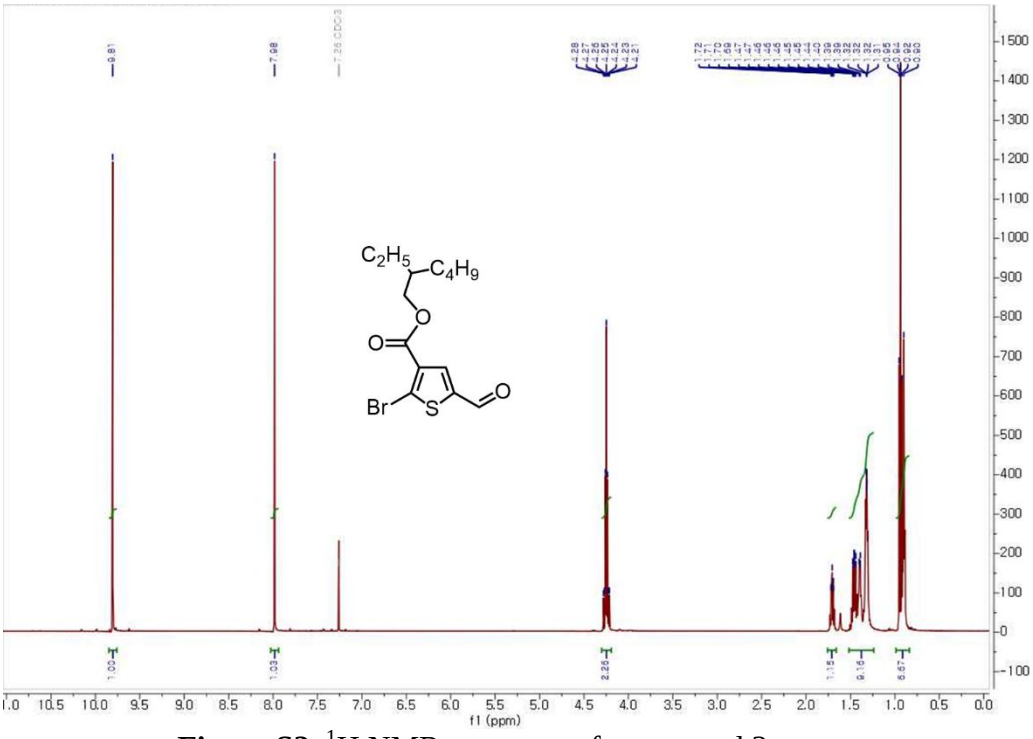

Figure S2. ^{1}H NMR spectrum of compound 3.

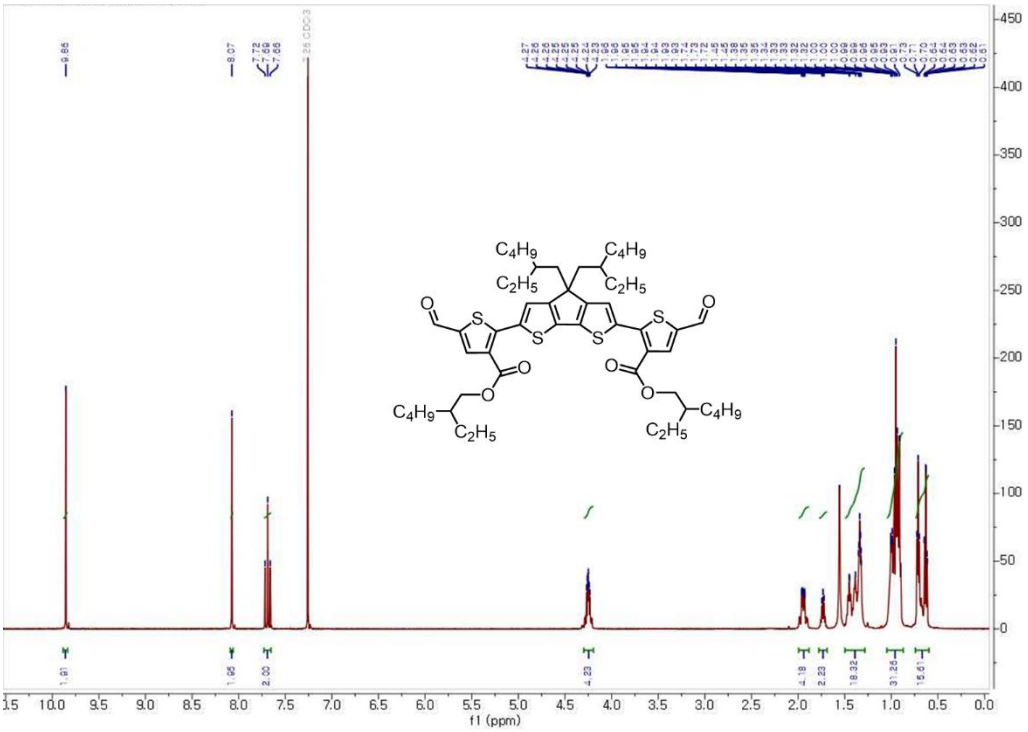

Figure S3. ^{1}H NMR spectrum of compound 5.

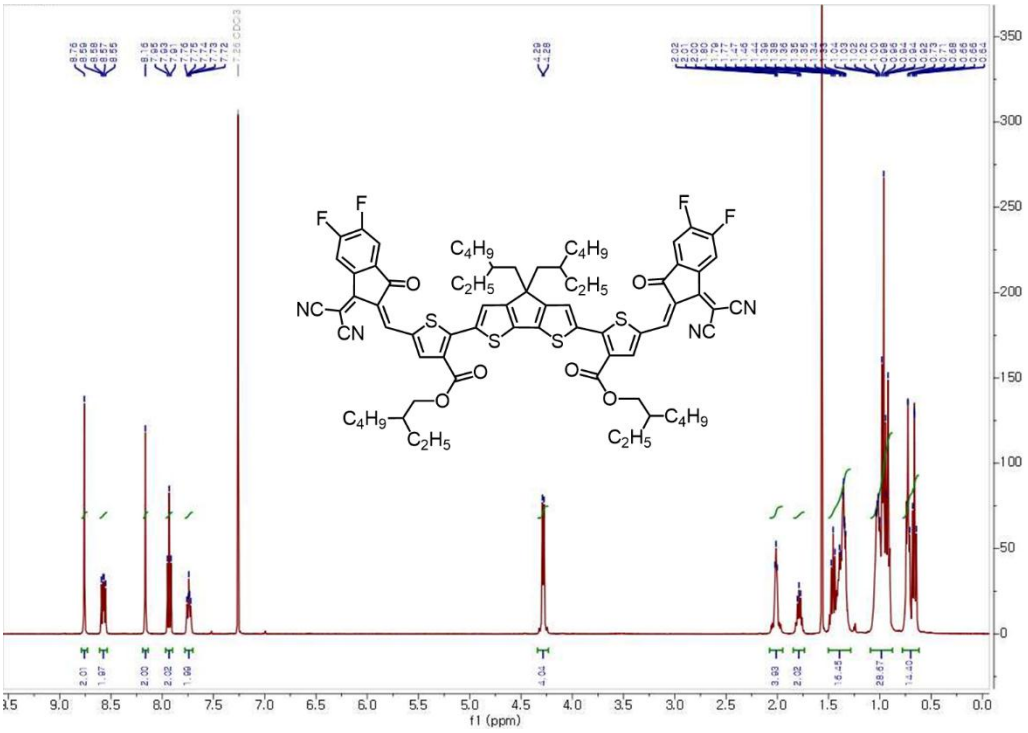

Figure S4. ^{1}H NMR spectrum of CETIC-4F.

Cyclic Voltammetry

Optical transitions determined from the onset of absorption lead to E_g^{opt} values of 1.34 ± 0.02 eV, 1.30 ± 0.02 eV, and 1.08 ± 0.02 eV for CETIC-4F, CTIC-4F, and COTIC-4F, respectively. Highest occupied molecular orbital (HOMO) and lowest unoccupied molecular orbital (LUMO) levels were estimated from the onsets of oxidation and reduction waves measured by cyclic voltammetry (Figure S5). The estimated HOMO/LUMO energy levels of CETIC-4F, CTIC-4F, and COTIC-4F are therefore −5.47 ± 0.04, −5.36 ± 0.04, and −5.22 ± 0.04, as well as −4.13 ± 0.04 eV, −4.06 ± 0.04 eV, and −4.14 ± 0.04 eV, respectively (Figure 1). We observed that an incorporation of the alkoxy substituents leads to a substantial red shift in the absorption maximum from 970 nm, and then to 1100 nm.

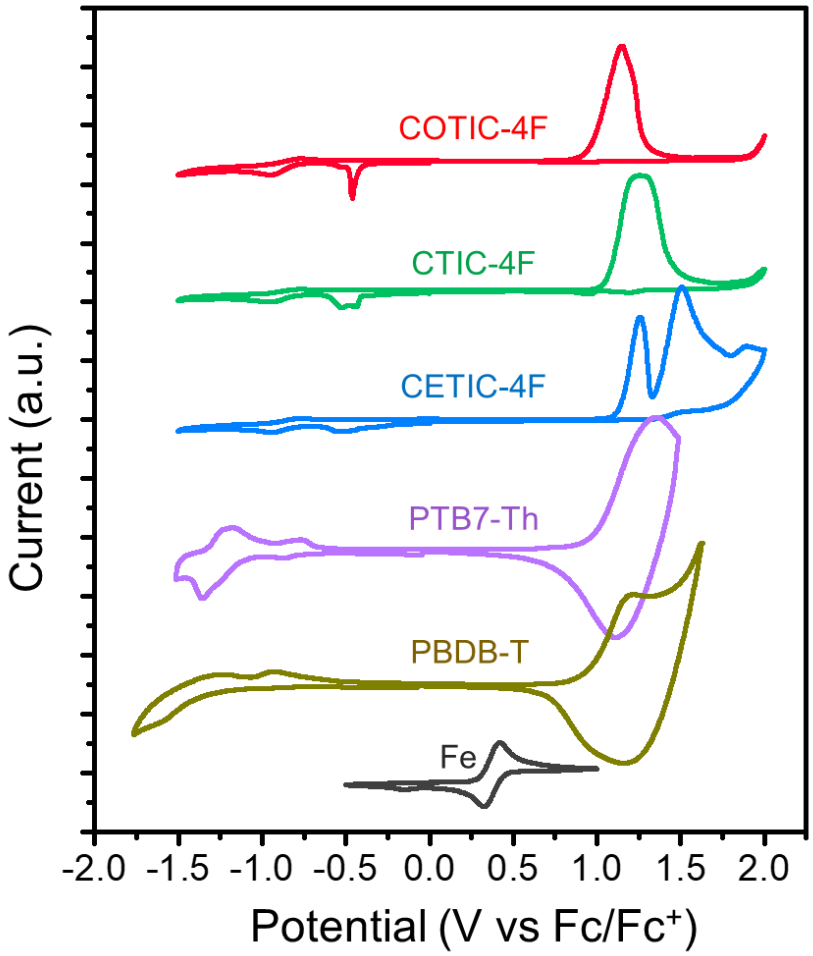

Figure S5. Cyclic voltammograms of the NFAs CETIC-4F, CTIC-4F, COTIC-4F, and the donor polymers PBDB-T, and PTB7-Th.

2. Device Fabrication and Analysis

Optimization and characterization of organic solar cells

Organic solar cells were fabricated to investigate the photovoltaic performance of the different donors and NFAs, namely PBDBT and PTB7-Th as well as CETIC-4F, and COTIC-4F. The following architecture was used for the investigated devices: ITO/ZnO/Donor:NFA/MoO_3/Ag. First, the ITO-coated glass substrates were cleaned with detergents, then sonicated in acetone and isopropyl alcohol and dried in an oven at 130 °C. The zinc oxide (ZnO) solution was prepared using a mixture of diethyl zinc and tetrahydrofuran (THF) (1:2, v/v %) and the ZnO film (35 nm) was prepared from spin-casting at 4000 rpm for 15 s and annealing at 110 °C for 15 min.[3,4] For deposition of the active layer, blend solutions of PTB7-Th (1 wt%):NFAs (1.5 wt%) dissolved in CB (with 2 vol% 1-chloronaphthalene, CN) were spin-coated on top of the ZnO layer in a nitrogen-filled glove box.[4] The best performance for devices using PBDBT as the donor were achieved with PBDBT:NFA ratios of 1:1 (wt%) with CB as the solvent and 2 vol% CN as processing additive. The devices were then pumped down in vacuum ($p < 10^{-6}$ torr; 1 torr ~133 Pa), and a 7 nm thick MoO_3/100 nm thick Ag electrode was deposited on top of the active layer by thermal evaporation. The deposited MoO_3/Ag electrode defined the active area of the solar cells as 22 mm^2. Photovoltaic characteristics measurements were carried out inside the glove box using a high quality optical fiber to guide the light from the solar simulator equipped with a Keithley 2635A source measurement unit. *J-V*-curves were measured under AM 1.5G illumination at 100 mW/cm^2 using an aperture (9.4 mm^2) to define the illuminated area. Neutral density filters were used to measure at lower light intensities (I = 100, 50, 25, 10 mW/cm^2). EQE measurements were conducted in a nitrogen-filled glove box using an EQE system. The monochromatic light intensity was calibrated using a Si photodiode and chopped at 100 Hz.

Capacitance spectroscopy

Capacitance spectroscopy measurements were performed with an impedance analyzer Solartron 1260A in the dark and under 1 sun AM1.5 illumination inside a nitrogen-filled glovebox. The amplitude of the AC signal was 40 mV to ensure a negligible impact on the measured impedance.

Open-Circuit-Voltage-Decay

The V_{OC}-decay measurements were performed with devices encapsulated with two-component epoxy outside of the N_2-filled glove box. The devices were illuminated by a fast switching light source (white LED) and once the illumination was turned off, the decay of the V_{OC} was monitored with the help of an oscilloscope connected via a high impedance buffer to ensure the necessary sub-microsecond time resolution of the measurements under open-circuit conditions. Due to the high impedance buffer, it can be assumed that the decay of the V_{OC} over time is only due to recombination taking place within the tested solar cells under high level of excitations. The intensity of the white LED was set to a value of 100 mW/cm^2. The measurement setup was inside of a faraday cage to ensure proper grounding.

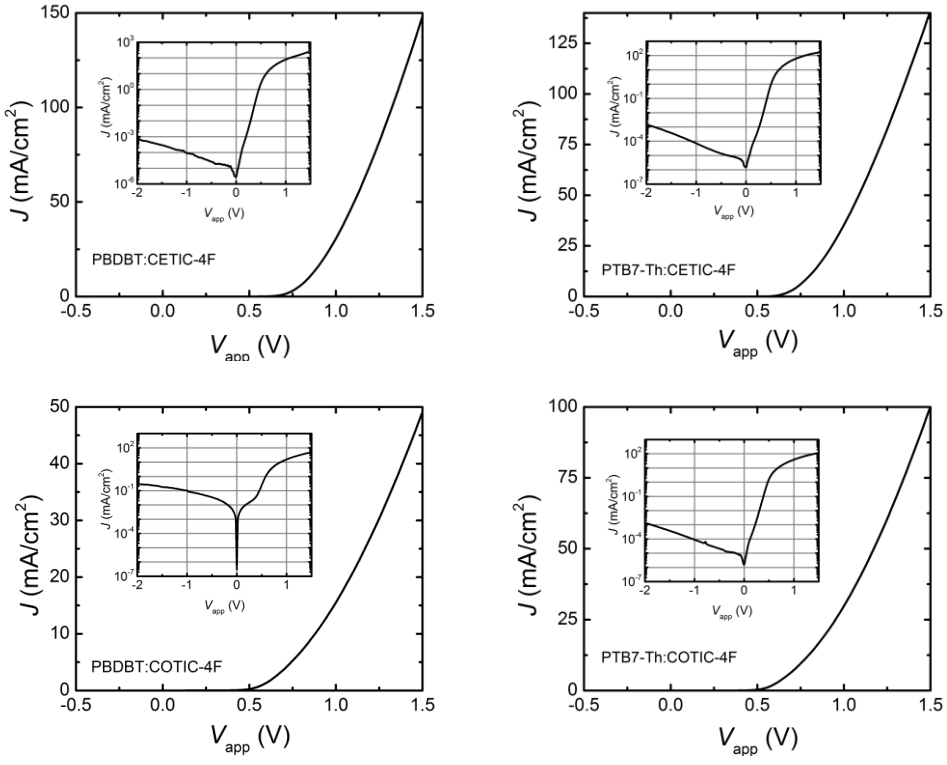

Figure S6. *J-V*-characteristics of the tested solar cells in the dark.

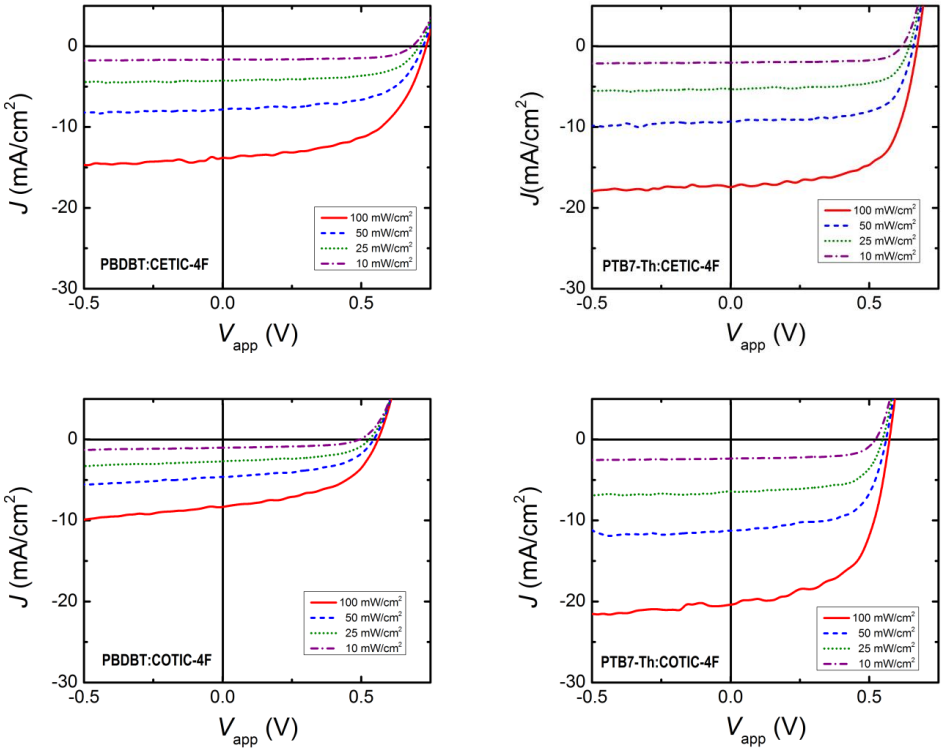

Figure S7. *J*-*V*-characteristics of the tested solar cells at different light intensities.

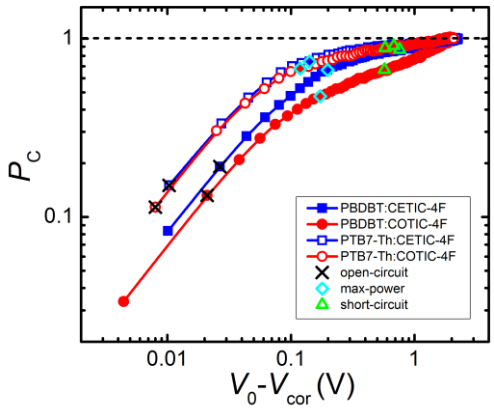

Figure S8. Collection probability P_C plotted against the effective voltage V_0-V_{cor}. The probability P_C at open-circuit, short-circuit, and maximum-power conditions is highlighted.

Table S1. Collection probability P_C determined at open-circuit (oc), maximum-power (mp), and short-circuit (sc) conditions. The PCEs are also listed for comparison.

Donor	NFA	P_C at **oc** [%]	P_C at **mp** [%]	P_C at **sc** [%]	$PCE_{avg\ (max)}$ [%][a)]
PBDBT	CETIC-4F	19.2	66.7	75.8	5.96 ± 0.77 (6.59)
	COTIC-4F	13.2	47.5	66.9	2.19 ± 0.12 (2.32)
PTB7-Th	CETIC-4F	15.1	74.4	91.1	7.61 ± 0.33 (8.08)
	COTIC-4F	11.4	67.9	88.8	6.66 ± 0.17 (7.04)

[a)] Average values from 10 devices

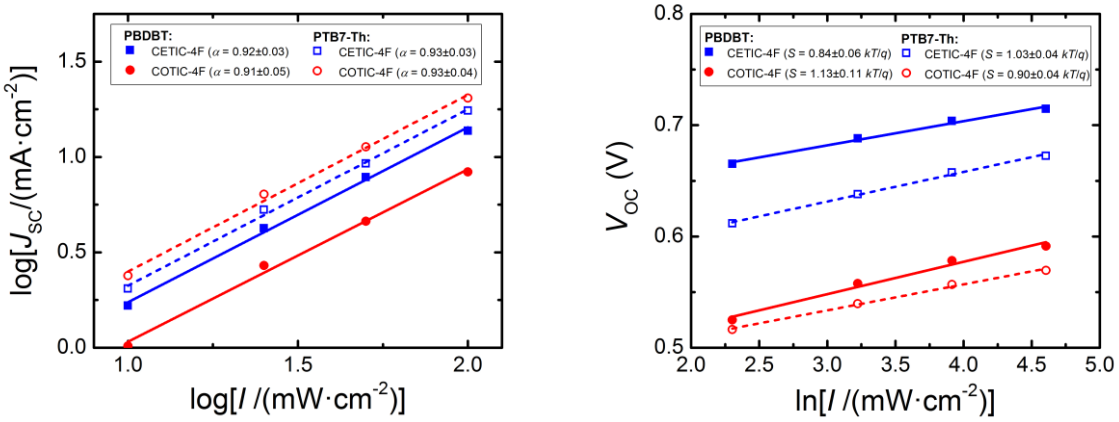

Figure S9. Light intensity dependent short circuit current density and open circuit voltage for the tested devices.

The electron and hole mobility $\mu_{e,h}$ of the donor-acceptor blends are determined by fitting the experimental results of the single carrier devices according to the Mott-Gurney law:

$$J = \frac{9}{8}\varepsilon_0\varepsilon_r\mu_{e,h}\frac{(V_{cor}-V_{bi})^2}{L^3}, \quad \text{(S1)}$$

where J is the current density, ε_0 is the vacuum permittivity, ε_r is the dielectric constant of the blend, V_{cor} is the voltage corrected for the losses due to the series resistance, V_{bi} is the built-in voltage, and L is the thickness of the active layer.

The dielectric constant ε_r of the blends was measured by capacitance spectroscopy at reverse bias and in the dark (Figure S10). In this case, there should be no frequency dependence of the capacitance. Then, the assumption is that the capacitance of the blends C_b measured under these conditions is equal to the geometric capacitance C_g, which would allow employing the following equation to calculate the dielectric constant ε_r:

$$\varepsilon_r = \frac{C_g L}{\varepsilon_0 A}, \quad \text{(S2)}$$

where L is the thickness of the active layer and A is the area of the device (A = 0.22 cm^2). The different blends have dielectric constants in the range of ε_r = 2.6 – 3.5 (Table S2).

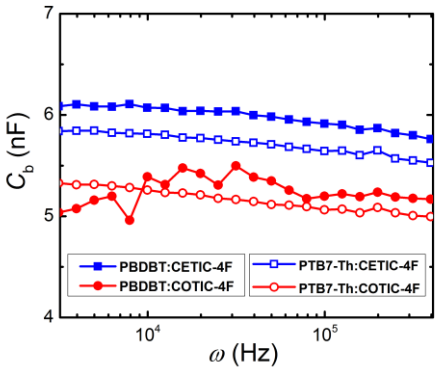

Figure S10. Capacitance of the different blends in the dark at different frequencies that were used to determine the geometric capacitance C_g.

Table S2. Geometric capacitance C_g, dielectric constant ε_r, built-in voltage V_{bi}, and electron/hole mobility $\mu_{e/h}$ determined for the studied blend systems.

Donor	NFA	L[a)] [nm]	L_{el}[a,b)] [nm]	C_g [nF]	ε_r	V_{bi}[c)] [V]	μ_e [cm^{2}V^{-1}s^{-1}]	μ_h [cm^{2}V^{-1}s^{-1}]	μ_h/μ_e
PBDBT	CETIC-4F	99.0	79.0	6.00±0.09	3.05±0.18	0.086	(7.98±0.13)·10^{-6}	(3.80±0.04)·10^{-5}	5
	COTIC-4F	100.2	83.0	5.26±0.14	2.71±0.18	0.042	(3.77±0.11)·10^{-6}	(5.20±0.13)·10^{-4}	138
PTB7-Th	CETIC-4F	91.5	69.0	5.73±0.09	2.69±0.18	0	(4.68±0.04)·10^{-6}	(5.91±0.08)·10^{-4}	126
	COTIC-4F	98.2	115.0	5.17±0.10	2.61±0.17	0	(3.80±0.01)·10^{-5}	(1.81±0.04)·10^{-3}	48

[a)]The thickness measurements are assumed to all have an error of ±5 nm. [b)]The hole only devices have the same thickness as the studied solar cells (L), whereas the electron only devices have the thickness L_{el}. [c)]For the electron only devices with PBDBT values for V_{bi} larger than zero had to be used for a successful fit, whereas for all other fits V_{bi} = 0 V was used.

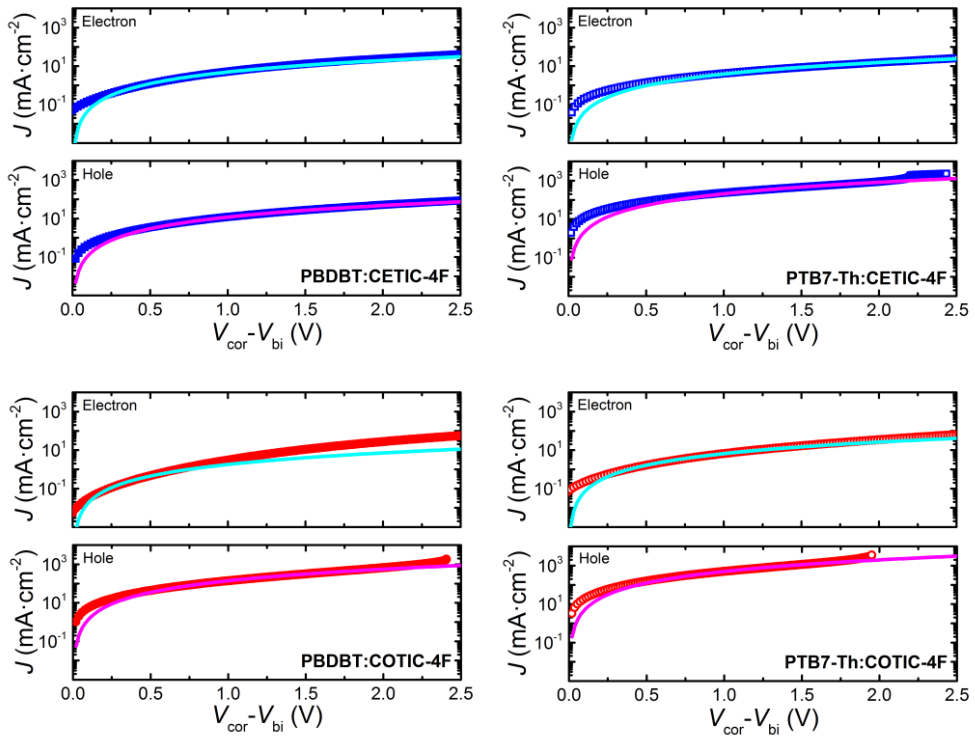

Figure S11. Mott-Gurney-plots of single carrier devices for the studied blend systems.

To begin a quantitative analysis of the recombination dynamics, it is necessary to obtain values for the charge carrier density *n*. It is known that capacitance spectroscopy can be employed to determine the density of charge carriers in organic solar cells under illumination. Capacitance spectroscopy was performed to yield the charge carrier density *n via* integration of the chemical capacitance ($C_{chem} = C_b[\omega = 400\ kHz] - C_g$) using the following equations:

$$n(V_{cor}) = n_{sat} + \frac{1}{qAL}\int_{V_{sat}}^{V_{cor}} C_{chem}\, dV_{cor}\,, \qquad \text{(S3)}$$

$$n_{sat} = \frac{1}{qAL} C_{sat}\,(V_0 - V_{sat}), \qquad \text{(S4)}$$

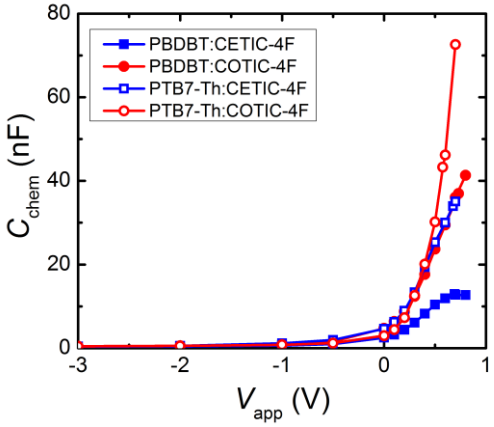

Figure S12. Chemical capacitance of the studied solar cells under AM 1.5G illumination at 100 mW/cm^2.

where *A* is the area of the solar cell, *L* is the thickness, V_{sat} is the reverse bias at which the photocurrent saturates, n_{sat} is the charge carrier density at the saturation voltage V_{sat}, and C_{sat} is the difference in capacitance of the BHJ layer C_b under illumination and in the dark at V_{sat} and an angular frequency $\omega = 400$ kHz. V_0 is the forward bias at which the photocurrent is equal to zero.

The calculation of a field and charge carrier dependent, effective mobility $\mu_{eff}(n,V)$ has been introduced by Albrecht et. al. as an alternative to the hole/electron mobility $\mu_{p/n}$ determined via the Mott-Gurney relationship of space-charge limited currents (SCLC) in single carrier devices.[5] It was argued that mobilities determined via SCLC measurements may be unreliable due to deviation from the expected thickness dependent behavior, the variation of electrode materials that may have an impact on the morphology, charge carrier densities and electric-fields that are larger in the SCLC regime in comparison to the normal operating conditions of a solar cell (ultimately leading to overestimated mobilities), and finally the fact

that the motion of injected carriers is measured in contrast to photogenerated carriers. The use of such an effective mobility μ_{eff} is especially encouraged, if a strong dependence of the mobility on either the applied bias V, the charge carrier density n, or both can be expected. The effective mobility μ_{eff} can be calculated by employing the following equation:

$$\mu_{eff}\left(n,V_{cor}\right)=\frac{J\left(V_{cor}\right)\cdot L}{2qn\left(V_{cor}\right)\cdot\left[V_{cor}-V_0\right]}\ , \tag{S5}$$

where J is the current density, V_{cor} is the corrected voltage, V_0 is the voltage at which the photocurrent is equal to zero, L is the device thickness, q is the elementary charge, and n is the charge carrier density obtained from capacitance spectroscopy.

The approach to reconstruct the recombination current density J_{rec} requires the charge carrier density n, effective mobility μ_{eff}, voltage, active layer thickness, and dielectric constant as input parameters and the reduction factor (ξ), the bulk trap density (N_{tb}), and the surface trap density (N_{ts}) as fitting parameters (Figures S13-S15).

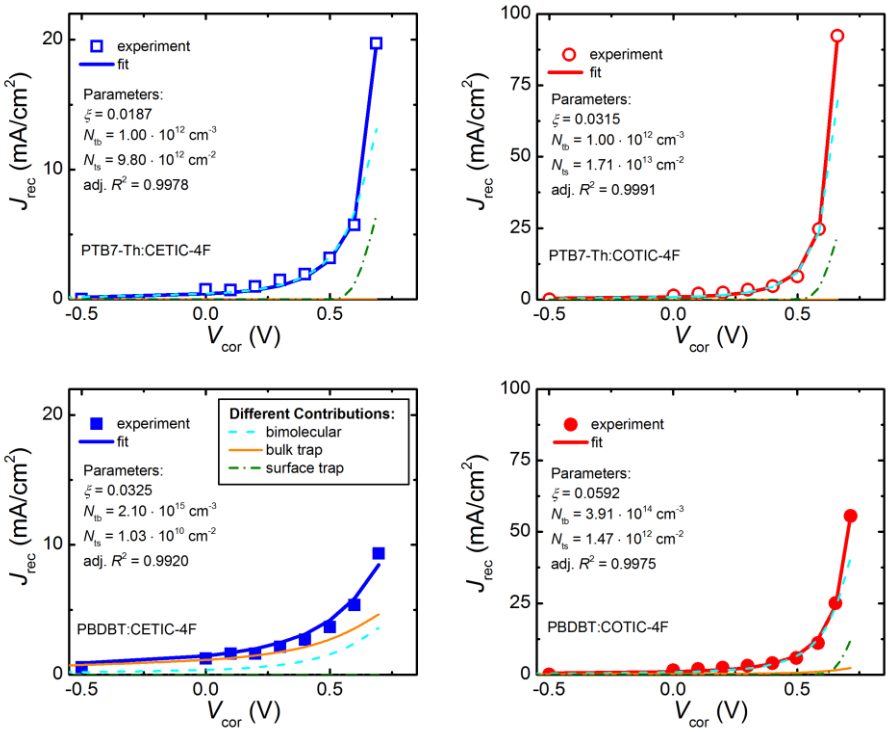

Figure S13. Experimental and fitted recombination current density J_{rec} of the different studied solar cells. The contributions from the different types of non-geminate recombination mechanisms are also presented.

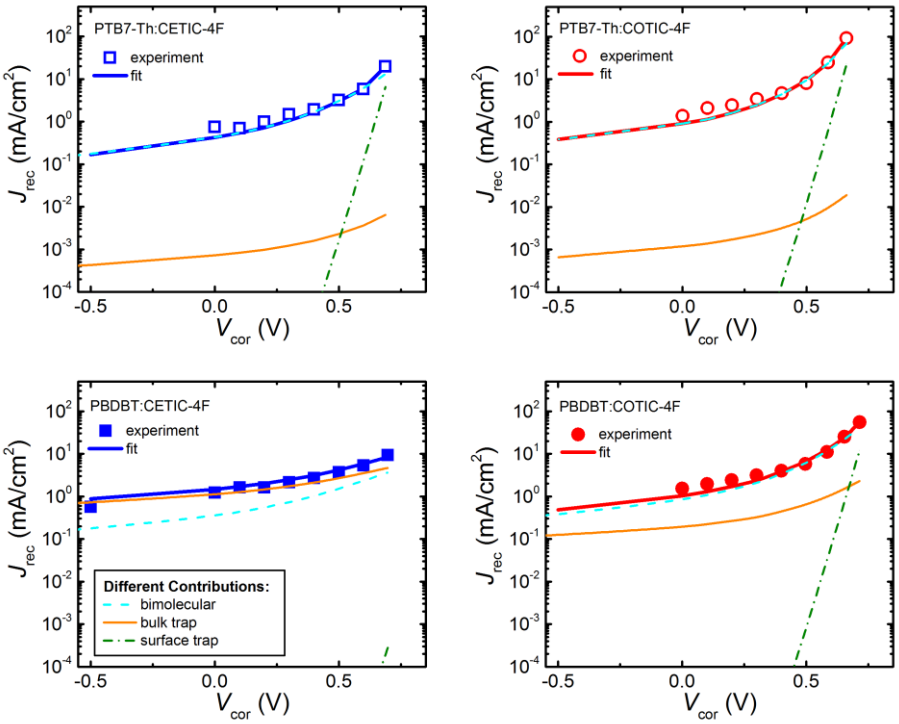

Figure S14. Experimental and fitted recombination current density J_{rec} of the different studied solar cells in semi-logarithmic scale.

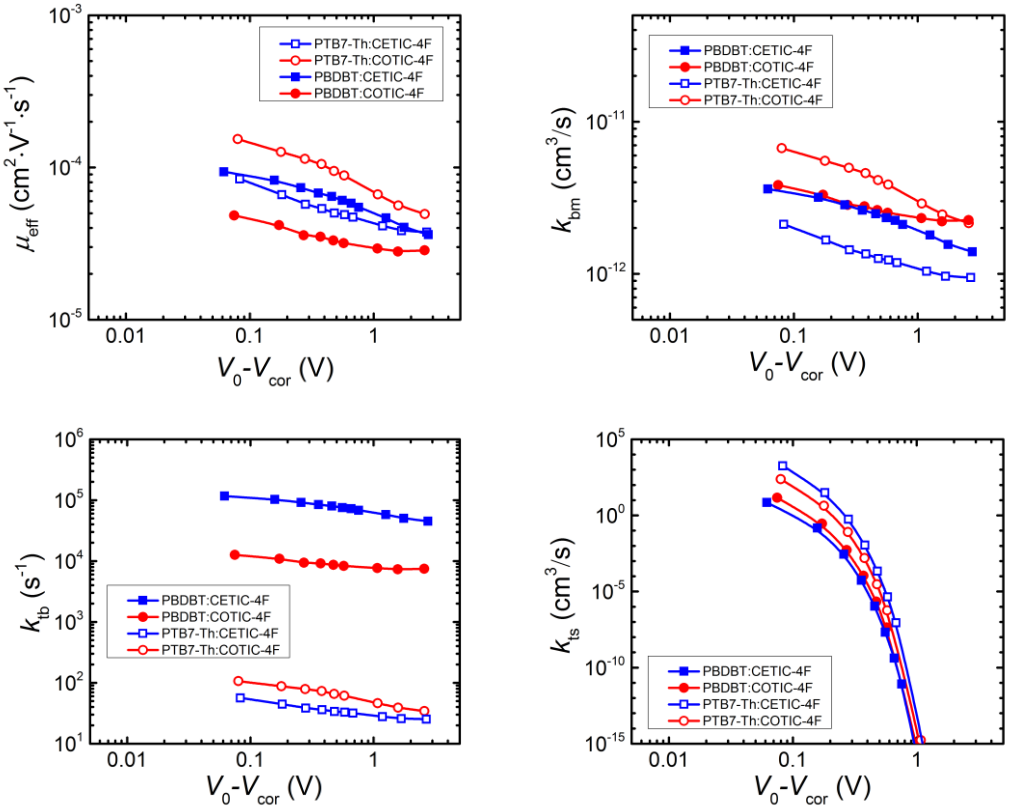

Figure S15. Effective mobility μ_{eff}, bimolecular recombination coefficient k_{bm}, bulk trap-assisted recombination coefficient k_{tb}, and surface trap-assisted recombination coefficient k_{ts} of the tested solar cells plotted as a function of corrected voltage.

The effective extraction τ_{ex} can be derived under the assumptions that a charge carrier will on average have to traverse half of the active layer thickness and that the active layer is assumed to be an effective medium. Then, the following two equations describing the drift velocity v_D have to be considered:

$$v_D = \mu\left|\vec{E}\right| = \mu\frac{V}{d}, \tag{S6}$$

$$v_D = \frac{d}{\tau_{ex}}, \tag{S7}$$

where μ is the charge carrier mobility, E is the electric field, V is the voltage, d is the distance, and τ_{ex} is the effective extraction time. By setting equations (S6) and (S7) equal and by solving for τ_{ex}, we obtain the following relationship:

$$\tau_{ex} = \frac{d^2}{\mu V} = \frac{L^2}{2\mu V} = \frac{L^2}{2\mu_{eff}[V_0 - V_{cor}]} = \frac{qLn}{J}, \tag{S8}$$

where the distance d was replaced by half the active layer thickness L, the mobility μ was replaced by the effective mobility ($\mu_{eff} = JL/(2qn[V_0\text{-}V_{cor}])$) and the voltage was replaced by the effective voltage $V_{eff} = V_0\text{-}V_{cor}$.

The following equation is the starting point for the analysis of the V_{OC}-transients:

$$R_{eff} = -\frac{dn}{dt} = -\frac{n}{\tau_{eff}} = k_{eff}n^{\beta}, \tag{S9}$$

where R_{eff} is the effective recombination rate, n is the charge carrier density, t is the time, τ_{eff} is the effective charge carrier lifetime, k_{eff} is the effective recombination coefficient, and β the effective recombination order. Similar to the reconstruction of the recombination current density *via* capacitance spectroscopy, it is assumed that the effective recombination rate R_{eff} is a superposition of different types of recombination mechanisms that do not directly influence one another – i.e. the recombination coefficients are independent from each other. Hence, the charge carrier lifetimes and recombination coefficients can be unraveled into the corresponding, separate contributions:

$$R_{eff} = R_{bm} + R_t = -\left(\frac{n}{\tau_{bm}} + \frac{n}{\tau_t}\right) = k_{bm}n^2 + k_t n. \tag{S10}$$

The different recombination orders of bimolecular (bm; $\beta = 2$) and of trap-assisted recombination (t; $\beta = 1$) have also to be taken into account. Furthermore, it has to be stressed that bulk and surface trap-assisted recombination cannot be distinguished by this method.

On the basis of Equation (S9) the recombination lifetime τ can be expressed as follows:

$$\tau = \frac{n}{R(n)} = \frac{1}{kn^{(\beta-1)}}. \tag{S11}$$

To access the recombination lifetime experimentally, Zaban *et. al*. derived an equation that relates τ to the transient V_{OC}, which is obtained *via* the V_{OC}-decay measurements:[6]

$$\tau = -\frac{kT}{q}\left(\frac{dV_{OC}}{dt}\right)^{-1}. \tag{S12}$$

Furthermore, the recombination order β can be determined using the following equation:

$$\beta = 1 + \frac{d\ln\tau^{-1}}{d\ln n} = 1 + \frac{kT}{q}\frac{d\ln\tau^{-1}}{d\ln V_{OC}}. \tag{S13}$$

It is possible to calculate the transient charge carrier density n_{OC} from the measured transient V_{OC} by applying the fundamental equation listed below:

$$n = \sqrt{n_i^2 \exp\left\{\frac{qV_{OC}}{kT}\right\}}, \tag{S14}$$

where n_i is the intrinsic charge carrier density.[7] The intrinsic charge carrier density n_i can be calculated by rearranging Equation S14, since the charge carrier density n at different biases, including V_{OC}, was already determined *via* capacitance spectroscopy. Subsequently, it is possible to calculate the transient n_{OC} from the measured transient V_{OC} *via* equation S14, once n_i is known.

In general, the effective recombination order β was calculated according to Equation S13 and it increases to local maxima of $\beta = 1.4 - 1.6$, which can be explained with the release of charge carriers from fast traps during the first microseconds and a combination of bimolecular and trap-assisted recombination under high excitation (Figure S16). Then, β decreases again to a value of $\beta \approx 1.0 - 1.2$, which indicates that the trap-assisted recombination starts to dominate at lower V_{OC}, and thus a lower charge carrier density n_{OC}. This behavior can be explained by the different dependence on charge carrier density n_{OC} for bimolecular and trap-assisted recombination.

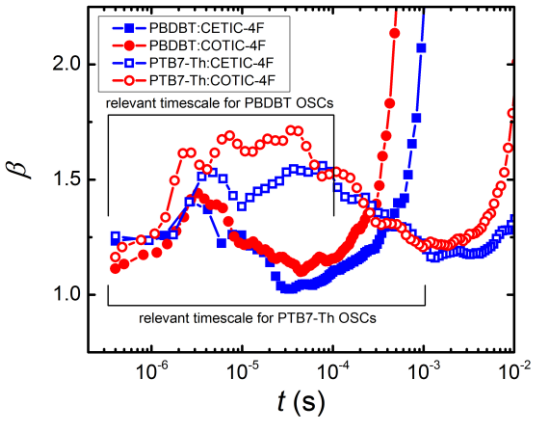

Figure S16. Transient evolution of the effective recombination order β for the studied OSCs.

Once timescales (PBDBT: $t > 10^{-4}$ s; PTB7-Th: $t > 10^{-3}$ s) of low levels of excitation are reached, β starts to steadily increase, surpassing even the local maxima of $\beta = 1.4 - 1.6$, phenomena which go beyond the described model.

3. Morphological Characterization

Grazing-incidence wide-angle X-ray scattering (GIWAXS)

GIWAXS measurements were performed at beamline 7.3.3 at the Advanced Light Source with an X-ray wavelength of 1.2398 Å at a 277 mm sample-detector distance. The measurements were calibrated using an AgB standard. Samples were scanned in a He environment at an incident angle of 0.12°.

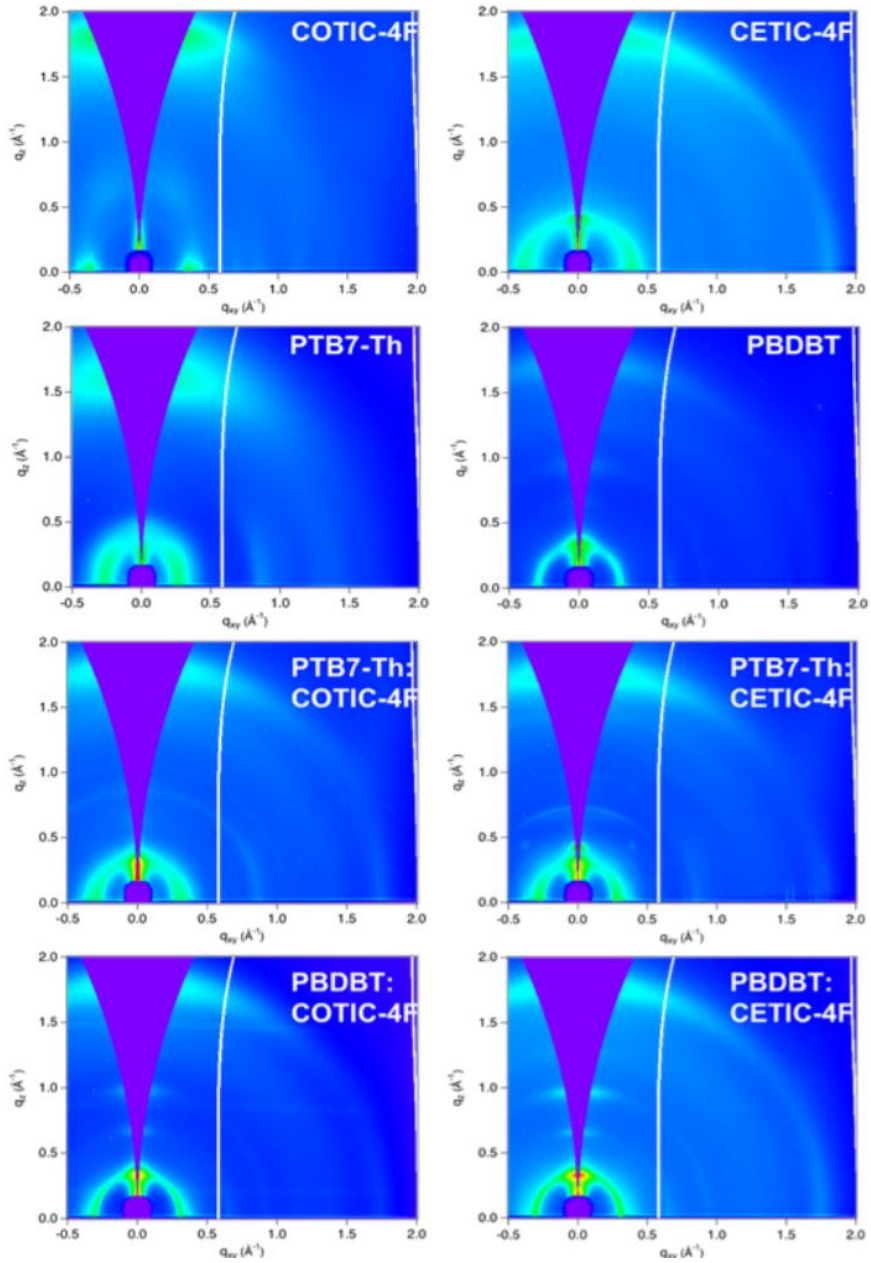

Figure S17. GIWAXS patterns of the different blend films used for solar cells, as well as GIWAXS patterns of the neat materials for reference.

Atomic Force Microscopy (AFM)

Atomic force microscopy (AFM) images were collected in air, using a silicon tip, and an Innova AFM operated under tapping mode.

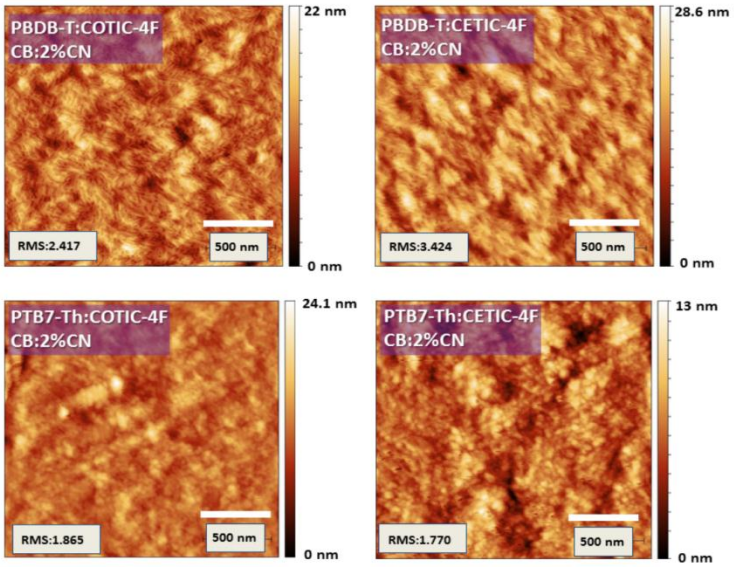

Figure S18. AFM height images of the different blend films used for solar cells.

References:

[1] G. C. Welch, R.C. Bakus, S. J. Teat, and G. C. Bazan, *Journal of the American Chemical Society*, *135*, 2298, 2013.

[2] Y. Sun, G.C. Welch, W. L. Leong, C. J. Takacs, G. C. Bazan, and A. J. Heeger, *Nature Materials*, *11*, 44, 2012.

[3] J. Lee, S.-J. Ko, M. Seifrid, H. Lee, B. R. Luginbuhl, A. Karki, M. Ford, K. D. Rosenthal, K. Cho, T.-Q. Nguyen, and G. C. Bazan, *Advanced Energy Materials*, *8*, 1801212, 2018.

[4] Jaewon Lee, Seo-Jin Ko, Hansol Lee, Jianfei Huang, Ziyue Zhu, Martin Seifrid, Joachim Vollbrecht, Viktor V. Brus, Akchheta Karki, Hengbin Wang, Kilwon Cho, Thuc-Quyen Nguyen, Guillermo C. Bazan, *ACS Energy Letters*, 4, 1401-1409, 2019.

[5] S. Albrecht, J. R. Tumbleston, S. Janietz, I. Dumsch, S. Allard, U. Scherf, H. Ade, D. Neher, J. Phys. Chem. Lett. 2014, 5, 1131.

[6] Arie Zaban, Miri Greenshtein, and Juan Bisquert, *ChemPhysChem*, 4(8):859–864, 2003.

[7] Simon M Sze and Kwok K Ng. *Physics of Semiconductor Devices*. Wiley Online Library, 2006.